Systems and Control Group

Thesis Systems and Control

Multi Cylinder Modelling of Broccoli Drying

Jaap Eisma

June 2010

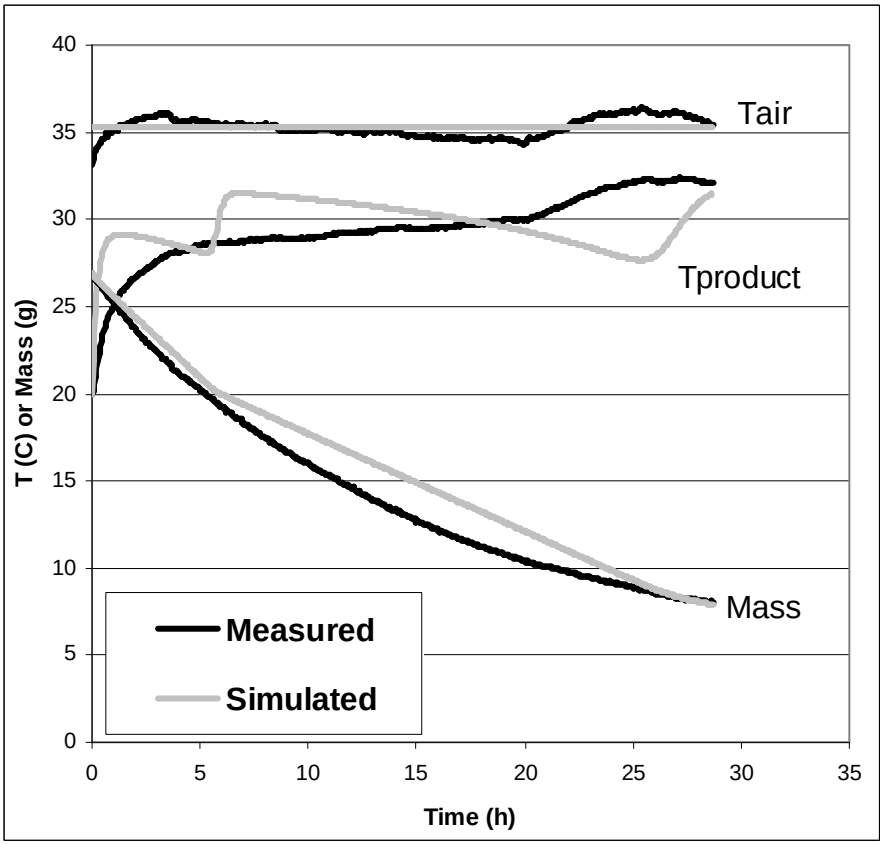

WAGENINGEN UNIVERSITY
AGROTECHNOLOGY AND
FOOD SCIENCES

Multi Cylinder Modelling of Broccoli Drying

Name course	:	Thesis project Systems and Control
Number	:	SCO-80436
Study load	:	36 ects
Date	:	June 2010

Student	:	Jaap Eisma
Registration number	:	86-11-22-219-100
Study programme	:	MFT (Food Technology)
Supervisor(s)	:	Xin Jin MSc Dr.ir. A.J.B. van Boxtel
Examiners	:	Dr.ir. K.J. Keesman,
Group	:	Systems and Control Group
Address	:	Bornse Weilanden 9 6708 WG Wageningen the Netherlands Tel: +31 (317) 48 21 24

WAGENINGEN UNIVERSITY
AGROTECHNOLOGY AND
FOOD SCIENCES

Abstract

Drying is a process that can be modelled according to the familiar rules of physics. In this thesis, drying of broccoli is modelled numerically using a multi-cylinder approach using the forward central formulation of Fick's second law on diffusion, with mass transfer equations as boundary conditions.

For broccoli dehydration, the model was adjusted according to several assumptions. These assumptions were drawn from results of practical experiments. Incorporation of shrinkage into the model was found to have no marked effect on the accuracy of model fits. Also, temperature gradients inside the product were ignored.

Heat transfer per mass unit ($W \cdot kg^{-1} \cdot K^{-1}$) was found to remain constant over the entire drying range. In addition to this, no significant influence of floret size or air temperature on this coefficient was identified. Air flow rate, on the other hand, was found to influence the heat transfer coefficient considerably.

From data fits performed over experimentally acquired data, parameter estimation delivered results which were compared to theoretical values.

From the comparison, the effect of the air flow temperature and surface area of the product were found to be in accordance with the theoretical values. Air flow rate proved difficult to predict. The cause of this may be found in oversimplification of air flow dynamics or the nature of the experimental setup.

Table of Content

List of Symbols

Symbol	Definition	Unit
a	cylinder quantity	-
A	contact area	m^2
a_w	water activity	-
C	water concentration	kg H2O/kg dry matter
c	conversion factor	-
c_p	specific heat capacity	$Jkg^{-1}K^{-1}$
D	diffusion coefficient	m^2s^{-1}
d	cylinder diameter	m
E_a	activation energy	$kJmol^{-1}$
F	pre-exponential factor	-
h	heat transfer coefficient	$Wm^{-1}K^{-1}$
h_a	heat transfer coefficient per surface area unit	
h_m	heat transfer coefficient analogue, per mass unit	
i	place denotation	
j	time denotation	
k	mass transfer coefficient	ms^{-1}
k_x	random reaction rate coefficient	
L	characteristic length	m
l	cylinder length	m
l_0	initial cylinder length	
M	mass	kg
M_0	initial mass	
M_{dm}	dry matter mass	
M_l	place-dependent mass	
M_p	product mass	
M_w	water mass	
n	cylinder type	-
Nu	Nusselt number	-
p_a	air vapour pressure	kgm^{-3}
p_p	product vapour pressure	kgm^{-3}
p_{sat}	saturation vapour pressure	kgm^{-3}
Pr	Prandtl number	-
r	cylinder radius	m
R	ideal gas constant	-
r_0	initial cylinder radius	m
Re	Reynolds number	-
Sh	Sherwood number	
t	time	s
T	temperature	K
T_a	air temperature	
T_p	product temperature	
u	air velocity	ms^{-1}
v_a	kinematic viscosity	m^2s^{-1}
V	volume	m^3
V_0	initial volume	
V_{dm}	dry matter volume	
V_{tot}	total volume	
V_w	water volume	
V_x	place-dependent volume	
x	random place determination	m
x_t	shrinking factor	-
ΔH	latent heat	$kJkg^{-1}$
η	dynamic viscosity of air	Pas
ρ	density	kgm^{-3}
ρ_0	initial density	
ρ_a	air density	
ρ_c	average density of composite	
ρ_{dm}	dry matter density	
ρ_w	water density	
Φ_h	energy transfer rate	Wm^{-2}
Φ_v	evaporation rate	$kgm^{-2}s^{-1}$

1 Introduction

Drying is classified as a molecular separation process in which water evaporates from the product. It has been applied to foods for a very long time. Lowering of water activity inhibits degradation of food by reduction of micro-organism growth as well as reduction of chemical reactivity. In addition to this, reduction of water content also results in reduction of product mass. This, in turn, reduces transportation costs.
Drying processes traditionally focus on achieving optimal demands regarding process economy and product quality. Process economy focuses on the rate at which water evaporates from a product and the energy efficiency of the entire process. Quality demands entail biochemical degradation of nutrients, loss of volatile (aroma) compounds and maintenance of product structure [1].
For solid products, convection drying is a frequently used approach. In this process air is used as a medium to carry water. The water concentration gradient between the air and the product ensures migration from the product to the air.

An ultimate goal in drying processes is enhancing the quality demands for convection drying by establishing a reduction of biochemical degradation of nutrients along with a decreased loss of aroma compounds.
In the investigation at hand, broccoli is chosen. It contains various vitamins, anti-oxidants and enzymes, all of which are assumed to be unstable upon heating. This allows for the identification of nutrient degradation. In addition to this, an interesting aspect of broccoli is its irregular shape, allowing little modelling simplifications.
The reactions rates under review are described by the Arrhenius equation, and therefore greatly temperature-dependent. So, when trying to reduce nutrient degradation, special attention needs to be paid to maintaining low temperatures throughout the process.

Modelling this process required a schematic depiction of the broccoli floret. Literature showed a potential solution: a collection of cylindrical shapes [2]. In chapter 2, Fick's second law and evaporative mass and heat transfer equations are applied to each of these cylinders.

For accurate modelling, insight into the drying process at low temperatures is needed. Chapter 3 features practical analysis of the drying properties: shrinkage, temperature gradients and shape maintenance. Experimental setups were developed to accurately monitor the evaporation rate as well as the temperature of the product. At the same time, air properties (temperature, flow rate and humidity) were documented. Processing at low temperatures, drying of broccoli was tracked over time.

In chapter 4, the numerical approximation of water concentration of all modelled cylinders is further elaborated on. Additionally, time and place discretisation are introduced and considered.

Subsequent chapters deal with the employment of the fitting a fitting program, estimation of diffusion and evaporation rate coefficients and their validation against theoretical values.

2 Model Theory

Physical Relations

During drying, of a number of processes occur: water diffusion, evaporation and heat conduction. Incorporation of these processes requires an equal number of physical equations.

Diffusion of water from the core of a sample towards the surface is given by Fick's second law:

$$\frac{\delta C}{\delta t} = D\frac{\delta^2 C}{\delta x^2} \qquad (1)$$

With C as water concentration (kg H_2O / kg dry matter) and D as diffusion coefficient ($m^{2}\cdot s^{-1}$).
Boundary conditions are translated to evaporation of water from the product to the surrounding air. This is described by the mass transfer equation:

$$\Phi_v = k \cdot \left(p_p - p_a\right) \qquad (1)$$

With Φ_v as the evaporation rate ($kg\cdot m^{-2}\cdot s^{-1}$), k as the mass transfer coefficient ($m\cdot s^{-1}$) and p_p and p_a as vapour pressure of the product-air interface and air respectively. The product vapour pressure is related to the water concentration through the water activity, in turn derived from the sorption isotherm. The sorption isotherm for broccoli is [1]:

$$a_w = 1 - e^{\left(-5.18 * C^{0.93}\right)} \qquad (3)$$

$$p_p = a_w \cdot p_{sat} \qquad (4)$$

Further details on vapour pressure calculations are explained in chapter 4.

Heat conduction can contribute to the presence of temperature gradients inside the drying product. These may determine the rate at which all processes occur, as D and k are temperature dependent. Heat conduction is described by Fourier's law:

$$\Phi_h = h \cdot \frac{dT}{dx} \qquad (5)$$

With Φ_h as the energy transfer rate ($J\cdot m^{-2}\cdot s^{-1}$), h is the heat transfer (conduction) coefficient ($W\cdot m^{-1}\cdot K^{-1}$).
The presence of temperature gradients can be identified with the Biot number:

$$Biot = \frac{h \cdot L}{k_C} \qquad (6)$$

With L as the characteristic dimension, typically described as volume per surface area (m) and k_C as thermal conductivity ($W \cdot m^{-1} \cdot K^{-1}$). Higher Biot numbers (> 0.1) indicate a large influence of conduction. Even inside the product, temperature gradients exist. For smaller Biot numbers (< 0.1), temperature gradients inside the product can be ignored.[3]

Multi-cylinder Model

To approximate the complex broccoli structure, literature offered the multi-cylinder model [4]. This model assumes that a floret is built up of branching cylinders. To narrow the size range for the different cylinders, 4 differently sized cylinders are defined (figure 1). Only radial diffusion is considered, lateral diffusion and evaporation are neglected. This allows further simplification of cylinders into one-dimensional geometries. Considering each cylinder as an individual shape allows uncomplicated cylindrical modelling. Adding of these separate shapes together produces the curve coherent with an entire floret.
Application of this model requires rewriting of Fick's second law to fit cylindrical coordinates [5]:

$$\frac{\delta^2 C}{\delta x^2} = \frac{1}{r} \cdot \frac{\delta}{\delta r} \cdot \left(r \cdot \frac{\delta C}{\delta r} \right) \qquad (7)$$

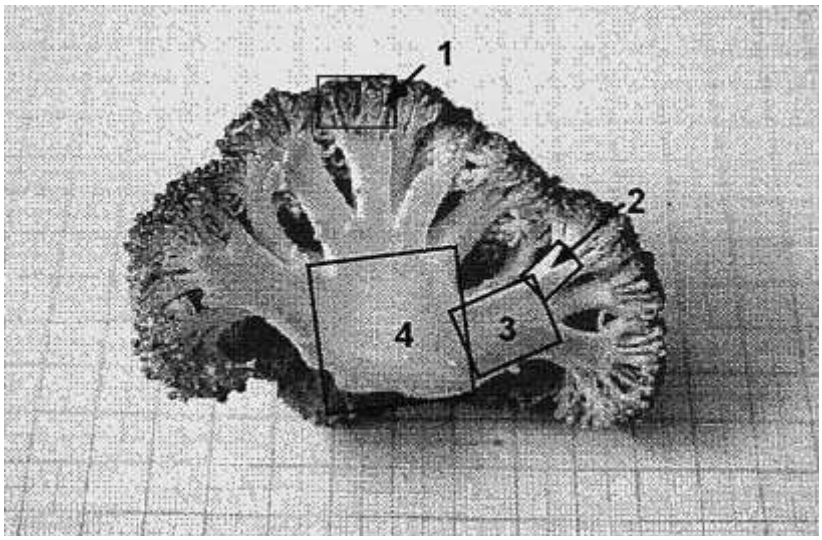

Figure 1. Schematic division of floret into cylinders. Adopted from Sanjuan et al. [4]

Sanjuan *et al.* mention average diameters, lengths, and mass percentage of the total floret mass of the 4 types of cylinders (table 1).

Table 1. Measurements of broccoli cylinders

Cylinder (n)	Diameter (d, cm)	Radius (r, cm)	Length (l, cm)	Weight percentage
Type 1	0.064	0.032	0.85	53.1
Type 2	0.31	0.155	0.47	7.7
Type 3	0.51	0.255	0.74	13.2
Type 4	1.75	0.875	1.23	26.0

From these figures, the amount of cylinders that should be added together to make up one entire floret is calculated.

$$amount_n \cdot \left(\pi \cdot r_n^{\,2} \cdot l_n\right) = [wt\%]_n \cdot M \qquad (8)$$

Setting the amount of type 4 cylinders to 1 results in 4 equations with 4 unknowns, which is solvable. This results in:

Table 2. Cylinder division, calculated from literature measurements

Cylinder	Indicative amount (a)
Type 1	2209.65
Type 2	24.70
Type 3	9.94
Type 4	1.00

In this result, an average size distributions is chosen, ignoring potential deviations. Therefore, it may be a little inaccurate. In addition, there is no back-up on this type of branching, from a plant science background. To complete the cylinder type assessment, the acquired figures are used in estimating figures which correspond to more common branching approaches.

For plant branching, more commonly applied approaches include exponential branching ($a = e^{X*N}$) and power branching ($a = N^X$), where N corresponds to 1 plus the number of previous branching splits.
Fitting power and exponential trend lines to the figures in table 2, with only 1 type four cylinder as a given ($a_4 = 1$), yields table 3 and figure 2. Models fitted with these cylinder divisions will be denoted by respectively “Exponent” and “Power”, whereas the figures obtained from the article will be denoted by “Sanjuan”.

Table 3. Cylinder divisions, using exponential and power branching.

Cylinder	Exponential	Power
X	2.4012	4.8879
Type 1	1344.26	876.62
Type 2	121.80	214.84
Type 3	11.04	29.61
Type 4	1.00	1.00

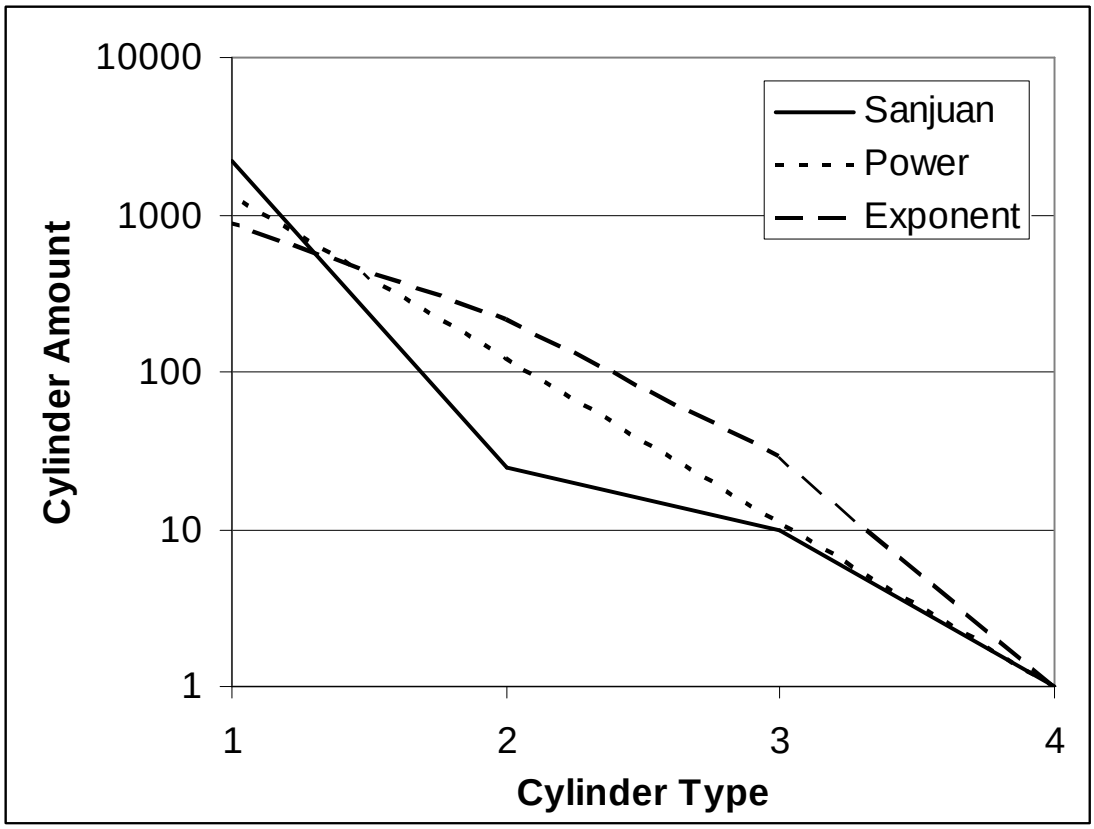

Figure 2. Comparison different cylinder divisions

Not every floret has the same size. It is, however, conceivable that the same shape is maintained on average. From this, the initial mass can be used to find the sizes of all 4 cylinder types:

$$M_0 = \left(a_1 \cdot r_1^{\,2} \cdot l_1 + a_2 \cdot r_2^{\,2} \cdot l_2 + a_3 \cdot r_3^{\,2} \cdot l_3 + r_4^{\,2} \cdot l_4\right) \cdot \rho_0 \cdot \pi \qquad (9)$$

Considering similar shapes, the diameter and length of any cylinder are related to the diameter and length of any other cylinder (Table 4). This means that equation 9 can be rewritten. By doing this, the radius of cylinder 4 can be expressed as a function of mass. From this, all cylinder measurements can be calculated.

Table 4. Relations between different cylinders

$r_1 = 0.064/1.75 * r_4$	$l_1 = 0.85/1.23 * l_4$
$r_2 = 0.31/1.75 * r_4$	$l_2 = 0.47/1.23 * l_4$
$r_3 = 0.51/1.75 * r_4$	$l_3 = 0.74/1.23 * l_4$
With	
$d_n = 2 * r_n$	$l_4 = 1.23/0.875 * r_4$

Modification of equation 9:

$$M_0 = \left(a_1 \cdot (t \cdot r_4)^2 \cdot u \cdot r_4 + a_2 \cdot (v \cdot r_4)^2 \cdot w \cdot r_4 + a_3 \cdot (x \cdot r_4)^2 \cdot y \cdot r_4 + (r_4)^2 \cdot z \cdot r_4\right) \cdot \rho_0 \cdot \pi \qquad (9b)$$

Where constants *t* through *z* represent conversion factors, as derived from table1.

Therefore: $r_4 = \left(\frac{M_0}{\left(a_1 \cdot t^2 \cdot u + a_2 \cdot v^2 \cdot w + a_3 \cdot x^2 \cdot y + z\right) \cdot \rho_0 \cdot \pi} \right)^{\frac{1}{3}}$ (9c)

Again applying conversion factors *t* to *z*, r_4 can be translated to all others radius and length values, each depending on the type of cylinder division used. For a typical floret of 30g, doing so delivers table 5.

Table 5. Cylinder geometry values obtained through multiple cylinder model

$\cdot 10^{-2}$ (cm)	Power	Exponent	Sanjuan
r_1	0.038	0.043	0.044
r_2	0.19	0.21	0.21
r_3	0.31	0.34	0.35
r_4	1.05	1.16	1.21
l_1	1.02	1.13	1.17
l_2	0.56	0.63	0.65
l_3	0.88	0.98	1.02
l_4	1.47	1.64	1.69

Shrinkage and Mass Calculation

Drying processes are characterised by product weight loss. Nearly all weight loss is accompanied by volume loss. In the model, this effect can either be incorporated or omitted. Both options can be argued:

A. Non-shrinking: dehydration is a cellular process. No matter how much the water content of the product decreases, on a biological level the same amount of cells take place in the diffusion process. These cells are only influenced by concentration gradients over their membranes. Diffusion does not show the characteristic response to volume decrease as physical equations suggest, making shrinkage an inappropriate contribution.

B. Incorporation: shrinking causes concentration gradients to be separated by smaller distances as the drying progress develops. Strictly physically speaking, this results in relative increase of diffusion rates. Therefore, the system requires shrinkage of spatial coordinates.

These different approaches require different methods of calculating product mass, both are outlined below.

A. No Shrinkage

The measuring procedure applied in the experiments (chapter 3) allows accurate mass measurements while the model focuses on water concentration of the product. In order to compare these results, moisture concentrations need to be converted to density (mass per cubic meter). Since the model does not shrink, density is a good measurement for mass loss due to mass transfer. In the following, density will be expressed as mass (M).
Total mass is divided over dry matter mass and water mass:

$$M_p = M_w + M_{dm} \quad (11)$$

Water mass is expressed as

$$M_w = C \cdot M_{dm} \quad (11b)$$

Therefore:

$$M_p = (C+1) \cdot M_{dm} \quad (11c)$$

Dry matter mass does not change at any point during drying and can be calculated from the starting values:

$$M_{dm} = (V_0 - V_0 \cdot [mass\%]_w) \cdot \rho_{dm} \quad (11d)$$

from:

$$M_{dm} = V_{dm} \cdot \rho_{dm} \quad (11e)$$
$$V_{dm} = V_0 - V_w \quad (11f)$$
$$V_w = V_0 \cdot [mass\%]_w \quad (11g)$$

where V_0 is the initial volume (set at $1m^3$), V_w and V_{dm} the volumes of water and dry matter at t = 0 respectively. M_{dm} is the dry matter mass per cubic meter of initial product, $[mass\%]_w$ the mass percentage of water at t = 0 and ρ_{dm} the dry matter density, the latter three were experimentally determined.

Multiplication of the product mass by the characteristic volume, determines the total mass.

$$M_l = V_x \cdot M_p \quad (12)$$

M_l is mass per predefined volume, V_x is the volume, further details on volume determination can be found in the numerical solution (chapter 4).

B. Shrinkage

The shrinking model is made up of a series of steps. Unlike the other model, this one includes a time dependent density. The steps taken to incorporate this shrinking process are:

1. Determine the initial cylinder dimensions.
2. Decide on a shrinking factor in relation to the volume loss.
3. Determine the composition of the remaining mass, thus calculating the product density.
4. Multiply the acquired shrunk volume by the product density to obtain product mass.

A drawback of this method is that the concentration of the previous time step in the numerical procedure is used to calculate the concentration at the next point as well as the relative dimensions. This results in a slight overestimation of product mass, as the density of the product increases every time step, while the volume decreases every next time step. However, provided the time steps are small enough, this phenomenon is negligible.

Step B.1 *Determine the initial cylinder dimensions.*
The dimensions of the cylinders at time 0 can be calculated through:

$$V_0 = l_0 \cdot \pi \cdot r_0^{\,2} \tag{13}$$

Step B.2 *Decide on a shrinking factor in relation to the volume loss.*
To simulate three-dimensional shrinkage, both radial and lateral shrinkage are incorporated (r and l respectively).
A shrinking factor (x_t) is determined through the following equation:

$$c \cdot V_t = x_t \cdot l_0 \cdot \pi \cdot \left(x_t \cdot r_0\right)^2 \tag{13b}$$

$$x_t = \left(\frac{c \cdot V_t}{l_0 \cdot \pi \cdot r_0^{\,2}} \right)^{1/3} \tag{13c}$$

The term c can be used to adjust dependency. Depending on the type of relation between water content and volume, the term c can be adjusted. Omission of the term describes a perfect linear relation between water content and volume.

Step B.3. *Determine the composition of the remaining mass, thus calculating the product density.*
The density of a product consisting of various composites (ρ_c) can be determined through

$$\rho_c = \frac{V_w}{V_{tot}} \cdot \rho_w + \frac{V_{dm}}{V_{tot}} \cdot \rho_{dm} = \frac{V_w \cdot \rho_w + V_{dm} \cdot \rho_{dm}}{V_{tot}} \tag{14}$$

With V and ρ as component volume and component density respectively. This results in:

$$\rho_c = \frac{\dfrac{C \cdot M_{dm}}{\rho_w} \cdot \rho_w + \dfrac{M_{dm}}{\rho_{dm}} \cdot \rho_{dm}}{\dfrac{C \cdot M_{dm}}{\rho_w} + \dfrac{M_{dm}}{\rho_{dm}}} = \frac{C \cdot M_{dm} + M_{dm}}{\dfrac{C \cdot M_{dm}}{\rho_w} + \dfrac{M_{dm}}{\rho_{dm}}} \tag{14b}$$

With

Water volume: $$V_w = \frac{M_w}{\rho_w} = \frac{C \cdot M_{dm}}{\rho_w} \quad (14c)$$

Dry matter volume: $$V_{dm} = \frac{M_{dm}}{\rho_{dm}} \quad (14d)$$

Step B.4. *Multiply the acquired shrunk volume by the product density to obtain product mass.*

$$M = \left(x_t \cdot l_0 \cdot \pi \cdot \left(x_t \cdot r_0\right)^2\right) \cdot \rho_c \quad (15)$$

At times, calculations may seem overly complicated. This is done because incorporation into the numerical system should be possible. (For further details on the incorporation into the numerical system, see chapter 4.)

3 Physical Property Determination

All of the previously discussed material is valid under any circumstance. In order to simplify the model to fit the broccoli drying process, some assumptions were made. To justify these assumptions, properties concerning temperature gradients, shrinking, and cylinder division were investigated. For this, experimental setups were developed. These will be discussed before further discussion on numerical model calculations and validation.

Experimental Setup

All drying experiments were performed in a convection dryer (figure 3). A convection dryer is a box with a product inside. This box has an air inlet and an air outlet. The humidity difference between the air and the product causes water to migrate to the air, which is then exported through the air outlet.

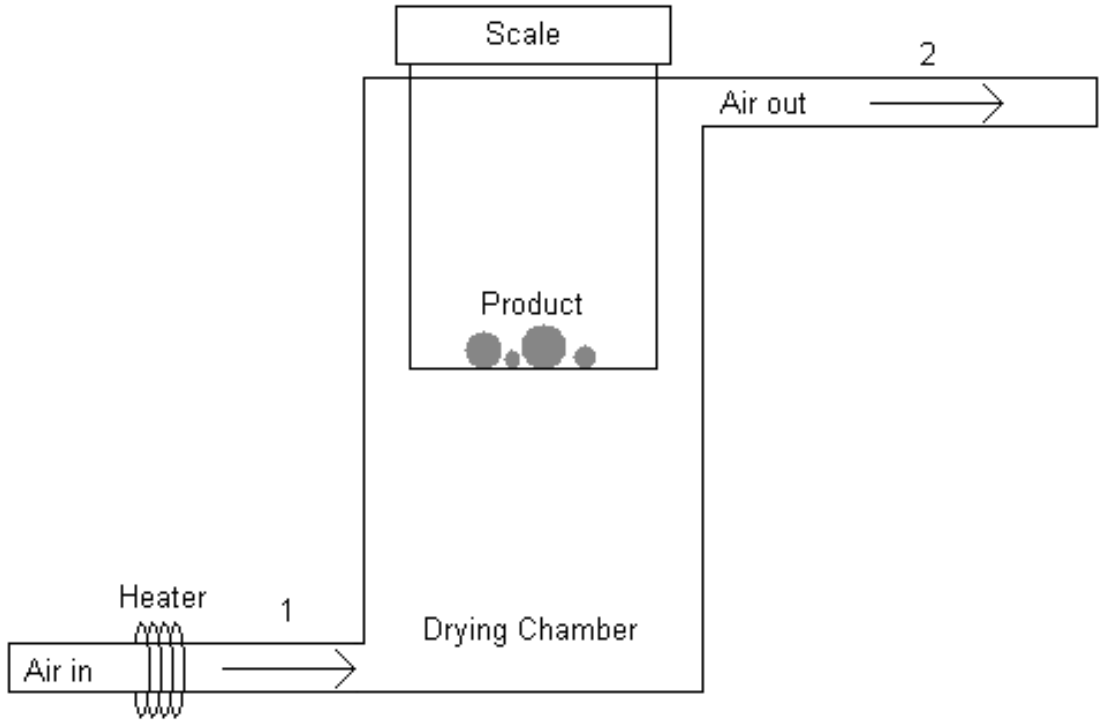

Figure 3, sketch of drying equipment

There are a couple of drying air properties which influence the drying process: air flow rate, air humidity and air temperature. In the experimental setup, the air humidity was not controlled, ambient air was used. The maximum attained air flow rate, was around a constant 0.23 $m \cdot s^{-1}$. For controlling the drying process, the setup qualifies: flow rate can be controlled, heating power can be controlled and air humidity can be monitored at several places.

The drying rate was measured. A non-invasive method was developed by introducing a data logged scale to the system. To inhibit the air flow inside from producing a noise signal on the measurements, the scale was placed outside the dryer. Using metal rods and a grate, the product was suspended from the scale.
Temperature change over time was also monitored. For online sample temperature measurements, data logged thermocouples were used. Thermocouples provide

accurate temperature measurement without microclimates and little lag in measurements.
Thermocouples work by introducing a wiring of different metals to a source and a reference temperature. Differences in temperature produce a small electric current. Measuring this current gives an accurate estimate of the temperature difference between source and reference.
Originally, this reference temperature was established by placement in an ice bath (T = 0°C) and ensuring equal temperature at voltmeter entrance by means of an isothermal block. Over the years, the ice bath reference has been replaced by a so called thermistor. This device offers resistance to the thermally induced current as a function of its temperature. This resistance is algorithmically translated to a measured temperature [6].
To measure a temperature gradient, differences between two points inside the product are more important than the actual temperature. For this purpose, a reference temperature is very useful. A dual-thermocouple was developed, enabling measurement of reference temperatures. If the reference temperature thermocouple is set to measure the temperature at the surface, while the source temperature thermocouple is set to measure the core temperature or vice-versa, the electric current will directly give information on the temperature difference. This current can easily be calculated to a temperature difference.
Thermocouples could be placed at any location in the drying chamber

Sample Preparation

For all experiments, broccoli of the strain *Brassica oleracea L.* were used. Slight variances in freshness of samples could not be excluded. Sealed packaging was used to minimise this variance.
Fresh broccoli florets were cut from the stem. To prevent unmodelled evaporation, cut surfaces were covered with petroleum jelly.
Samples were placed inside the drying chamber and dried for certain periods of time. During this time temperatures and flow rates were set. For the flow rates, ranges of 0 to 0.23 ms^{-1} were used. Temperatures ranged between 20 and 60 °C.

Shrinkage

During drying of broccoli, shrinkage was identified (figure 4). For many drying processes, product volume is considered as linearly dependent on water content. For a vegetable product like broccoli it is possible that the presence of fibrous components such as cell walls may result in a relation that is not entirely linear. The degree of linearity of this relation was calculated.

Figure 4,Shrinkage during drying. Left, a fresh broccoli floret. Right, a dried broccoli floret.

For reference, fresh samples were completely dried (100°C, 24 h) in duplicate to determine the initial water content.
42 samples of broccoli stem with varying mass (ranging between 3 and 6 g) were cut. In preparation, all samples were soaked overnight to make sure initial water concentrations were equal for each sample.
Drying proceeded over a range of 0 to 25 hours to obtain a wide range of water concentrations. Each sample was dried over three intervals. In the first interval, the time range was set, samples were dried for a varying period of time. The second and third interval , all samples were dried for an additional 8 hours.
After each interval, samples were stored in a confined space overnight to ensure even distribution of water.
The volume of the stored samples was measured by means of submersion. Provided this experiment is done fast enough. Submersion does not influence the water content of the sample significantly.

The results gathered from the experiment, give a linear relation ($\rho = -0.0013 \cdot C + 1.1218$, figure 5). Proof of this is the fact that this linear relation runs through a product density of 1.00 $kg \cdot L^{-1}$ at 100% moisture content.
In addition to the linear relation, the results offer a quantification of the dry matter density. At 0% water, a density of 1.12 $kg \cdot L^{-1}$ is found.

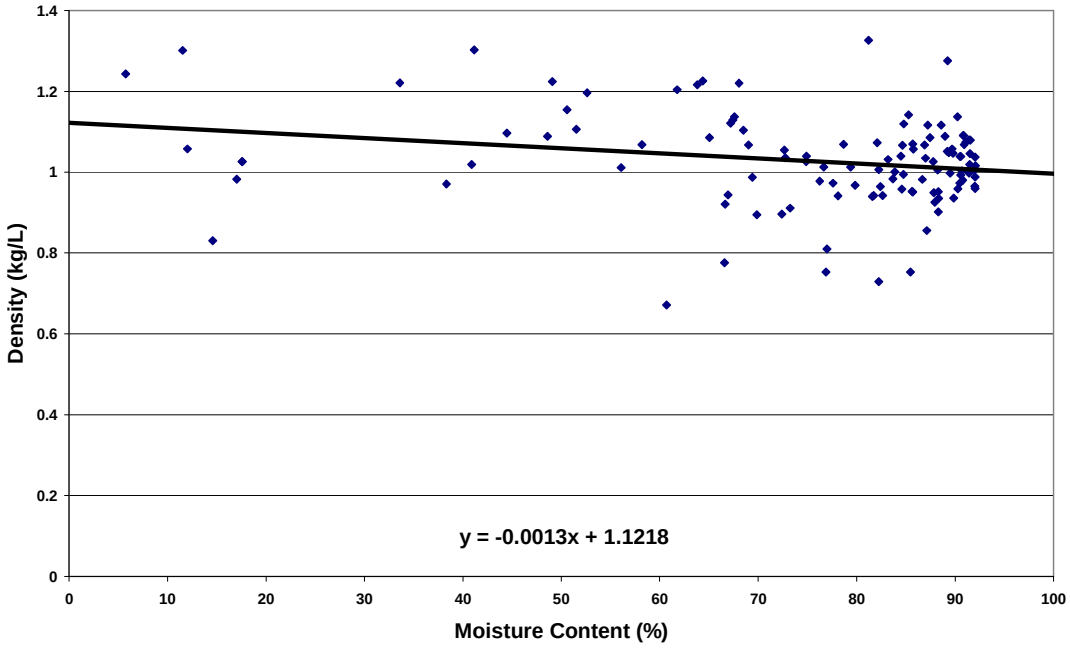

Figure 5. Product density at varying water content

Temperature Gradient

As stated previously, the degree of heat conduction determines temperature gradients. These may influence the rate at which reactions occur. The influence of potential temperature gradients was investigated.

Theory suggests that temperature gradients can be neglected for Biot numbers around 0.1 [3]. These bodies are defined as thermally thin.

The Biot number is a function of heat transfer coefficient, thermal conductivity and characteristic length ($L = V \cdot A^{-1}$). Since heat transfer coefficient and thermal conductivity of broccoli are still a point of research, typical vegetable values will be used. For the heat transfer coefficient these range from 40 to 90 $W \cdot m^{-1} \cdot K^{-1}$ [7]. For thermal conductivity, values range from about 0.5 to 0.6 $W \cdot m^{-1} \cdot K^{-1}$ [8]. To test the influence, worst case scenarios (highest heat transfer, lowest heat conductivity) were tested over a range of cylinder diameters (table 2). The figures are calculated for typical cylinder dimensions of l = 2d.

Figure 6. Worst case scenario Biot simulations

d (m)	V (m^3)	A (m^2)	L (m)	Biot
0.0025	2.45E-08	7.85E-05	3.13E-04	0.05625
0.005	1.96E-07	0.000314	6.25E-04	0.1125
0.01	1.57E-06	0.001257	1.25E-03	0.225
0.02	1.26E-05	0.005027	2.50E-03	0.45

These figures suggest that temperature gradients may be present in a drying floret. Therefore, an experimental evaluation was done.

Using four samples of relatively large florets (m > 40g, d_{base} = 1.5 – 2 cm), the heating process with an inflow of air at around 55°C was started. Placing the previously described dual-thermocouple for temperature gradients in the core and near the surface of a floret stem ($\Delta x \sim ½d$), a qualitative experiment was performed. This way approximate temperature gradients were identified.

Using these temperature gradients, differences in diffusion coefficient and nutrient degradation can be estimated. Both of these coefficients respond to temperature as described by the Arrhenius equation [1]:

$$k_x = F \cdot e^{-\frac{E_e}{R \cdot T}} \qquad (16)$$

With k_x as a reaction rate coefficient, A the pre-exponential factor, E_a the activation energy, R the ideal gas constant and T the product temperature (K).
From the Arrhenius equations, variations in diffusion and degradation coefficients were calculated over the drying range at hand (20 - 60°C). This variance was then calculated for the maximum temperature difference as obtained from measurements. As all values were compared on a relative level, pre-exponential factors were set at 1.

Measurements showed that, aside from the temperature adaptation phase, temperature differences are mostly below 1K (figure 7). The effects on degradation rate and diffusion coefficient are calculated in table 6.
Judging from these figures, it can be concluded that even though there certainly is some presence of a temperature gradient, the effect expressed as percentual difference over 1K does not even amount to 1% (right column). Effects of temperature can be neglected and no adaptation into the model is required.

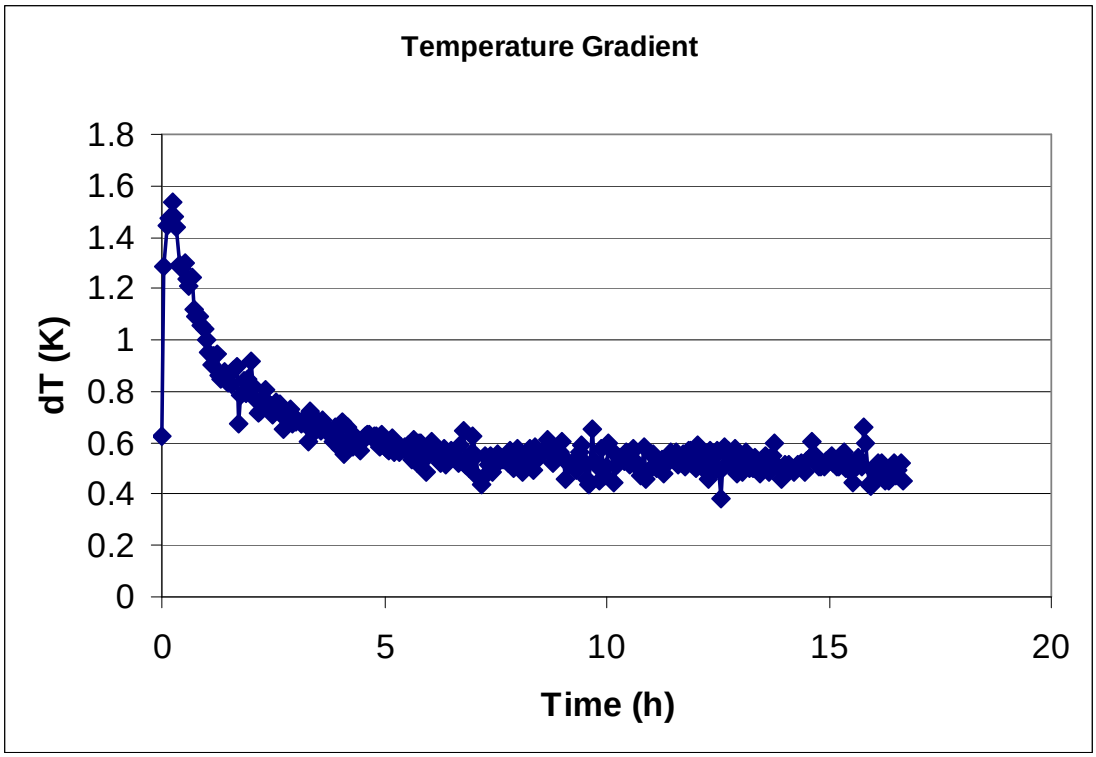

Figure 7. Sample with the biggest temperature gradient. Temperature differences between surface and core of a floret. Y-axis represents absolute temperature difference (K), X-axis drying times (s). Data points are weighted averages over 200 s.

Table 6. Influence of temperature gradient on rates

	Max Activation Energy ($E_{a,max}$, $kJmol^{-1}$)	Rate range over 40 degrees	Percentual rate difference ($\%K^{-1}$)
Diffusion Rate Coefficient (D [7])	18.5	0.89 – 0.96	0.06 – 0.52
Typical vitamin degradation (Vit. C [8])	19.0	0.95 – 0.98	0.03 – 0.3

Shape Maintenance and Heat Transfer

From measurements, a temperature difference between product and air flow was identified (figure 8). Since temperature gradients inside the product can not be the cause of this, heat transfer and evaporation rate were further investigated.

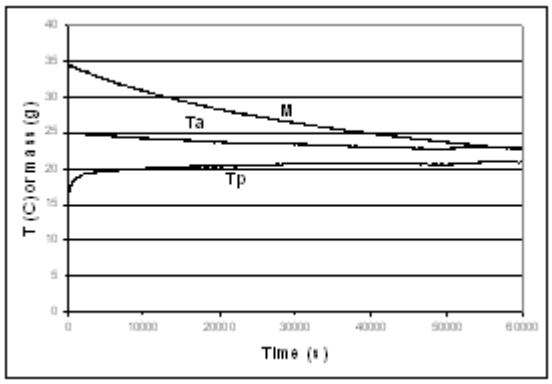

Figure 8. Measured values for mass (M), air temperature (Ta) and product temperature (Tp) of a drying broccoli floret.

The heat transfer coefficient is inherently linked to the surface area of a product, as identified by the heat transfer equation:

$$\Phi_h = h_a \cdot A \cdot (T_a - T_p) \tag{17}$$

In which Φ_h represents the heat flux, h_a the heat transfer coefficient and T_a and T_p the air and product temperature respectively.
The complex structure of broccoli makes it hard to determine the surface area accurately. Linking heat transfer to mass instead allows rewriting of equation 17:

$$\Phi_h = h_m \cdot M \cdot (T_a - T_p) \tag{18}$$

With h_m as substituted heat transfer coefficient and M as product mass.
This substitution is justified through assuming equality of shape for florets during drying.
Tracking of energy transfer along with the temperature of product and air flow, offers values for h_m.

For drying processes, there are two main processes that require energy: evaporation of water and heating up of the product. Total heat transfer is calculated by addition of the energy usage of these processes.
Division of the acquired h by initial product mass, produces the heat transfer coefficient.

$$\begin{aligned} &Heat\_transfer = evaporation + heating \Rightarrow \\ &h \cdot (T_a - T_p) = \Delta H \cdot \Delta M + \Delta T \cdot M \cdot c_p \end{aligned} \tag{19}$$

With T_a and T_p as air and product temperature, ΔH as latent heat of water (2256 $kJ.kg^{-1}$), M as product mass, ΔM as evaporated moisture, ΔT as temperature increase and c_p as the specific heat capacity (3890 $Jkg^{-1}K^{-1}$) of the product.
For a number of drying curves, the steps above were taken. Analysis showed estimates that are quite scattered. In this scattered data little time-dependency of h_m. In figure 9, this independency is shown.

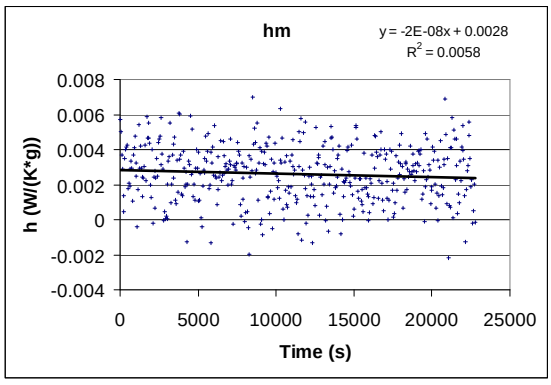

Figure 9. Independency of h_m on time throughout the drying process

Among different drying experiments, h_m is relatively constant, the expressions of y-intersects obtained from the results does not appear to be influenced by either temperature (μ=35.32°C, σ=11.92) or product mass (μ=27.64g, σ=5.45) as shown in

figure 10 and 11. Only the air flow rate (range ~ 0.04 – 0.23) influences the heat transfer coefficient. (figure 12). This can be explained through the Nusselt number.

$Nu = 0.664 \cdot \mathrm{Pr}^{1/3} \cdot \sqrt{\mathrm{Re}}$ with $Nu = \frac{h \cdot L}{\lambda}$, $\mathrm{Pr} = \frac{v_a}{a}$ and $\mathrm{Re} = \frac{\rho \cdot u \cdot L}{\eta}$

Gives:

$$h = \frac{\lambda}{L} \cdot 0.664 \cdot \mathrm{Pr}^{1/3} \cdot \sqrt{\mathrm{Re}} \qquad (20)$$

With L as characteristic dimension and λ as thermal conductivity [9].
In this equation, L (characteristic length) is influenced by mass, u (air velocity) is influenced by air flow rate and v_a (kinematic viscosity), ρ_a (air density) and η (dynamic viscosity of air) are influenced by temperature (appendix 2).
The equation above can be simplified for assessment of influence of individual process parameters:

Table 7. Effect of individual process parameters on heat transfer.

Parameter	Mass	Air flow rate	Temperature
Influence	$M = c \cdot L$		v_a and η from various tables (appendix 3) $\rho_a = 360.77819 \cdot T^{-1.00336}$
Reduced expression	$h = \frac{1}{L} \cdot c \cdot \sqrt{L}$	$h = c \cdot \sqrt{u}$	$h = c \cdot v_a^{1/3} \cdot \sqrt{\frac{\rho}{\eta}}$

With c as a combination of constants related to independent air and product properties and u as the air flow rate.

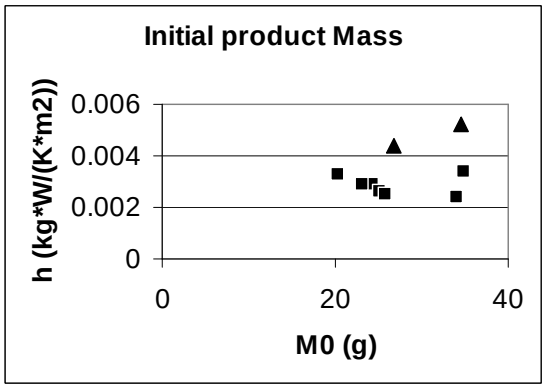

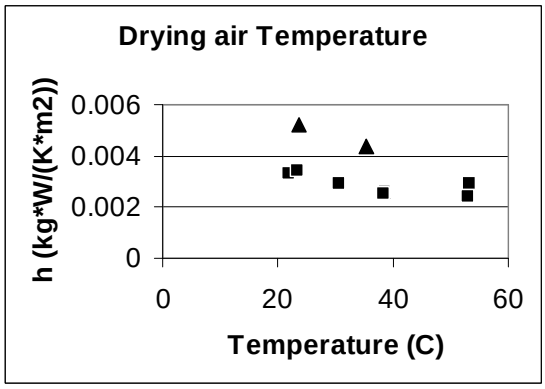

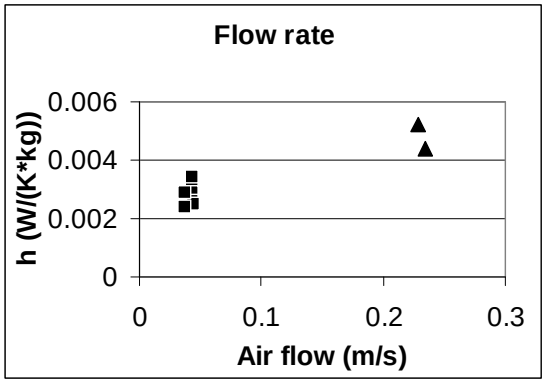

Figure 10, top left. hm is independent of mass. Triangles represent deviating values.

Figure 11, top right. hm is independent of temperature. Triangles represent deviating values.

Figure 12, bottom. Flow rate determines hm. Triangles represent deviating values.

The effect of the temperature and initial mass range did not produce significantly different values for h_m, while the air flow range did.
In order to produce significant differences, mass values should either be smaller than 15g or larger than 37g. Temperatures should be lower than 2°C or higher than 65°C. Both of these ranges are equal to the ranges used in this research.

The tendency towards to theoretical value confirms the validity of the assumption of equal shapes for different florets.

4 Numerical Solution

General Model

The entire programming file is included in appendix 1.

Diffusion modelling of infinitely long cylinders is defined by the modification of Fick's law:

$$\frac{1}{D}\cdot\frac{\delta C}{\delta t}=\frac{1}{r}\cdot\frac{\delta}{\delta r}\cdot\left(r\cdot\frac{\delta C}{\delta r}\right) \qquad (7b)$$

For a numerical solution, rewriting is essential. The forward central scheme with time denotation "j" and place denotation "i" yields:

$$\frac{C_{i,j}-C_{i,j-1}}{D\cdot\Delta t}=\left(\frac{r_{i+0.5}\cdot\left(\frac{C_{i+1,j-1}-C_{i,j-1}}{\Delta r}\right)-r_{i-0.5}\cdot\left(\frac{C_{i,j-1}-C_{i-1,j-1}}{\Delta r}\right)}{r_i\cdot\Delta r}\right) \qquad (21)$$

$$\frac{C_{i,j}-C_{i,j-1}}{\Delta t}=\frac{D}{r_i\cdot\Delta r^2}\cdot\left(r_{i+0.5}\cdot C_{i+1,j-1}-\left(r_{i+0.5}+r_{i-0.5}\right)\cdot C_{i,j-1}+r_{i-0,5}\cdot C_{i-1,j-1}\right) \qquad (21b)$$

With $r_{i+0,5}=\frac{r_i+r_{i+1}}{2}$ and $r_{i-0,5}=\frac{r_i+r_{i-1}}{2}$ for central differences.

This implies that the calculation of a concentration at place i at time j, is dependent of the concentrations of points i-1, i and i+1 at time step j-1 (figure 13).
This method can be illustrated by a layered geometry (figure 14).

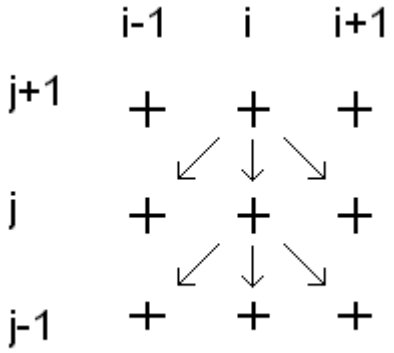

Figure 13. Pluses represent concentration values, arrows indicate the dependency on each other.

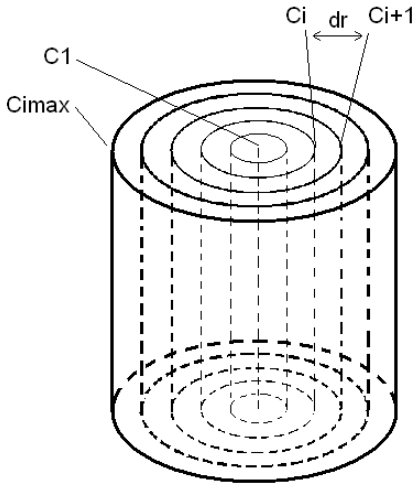

Figure 14. Schematic depiction of a cylinder of broccoli. C as concentration, i as place numerator and dr as δr. 1 and imax are the boundaries, further discussed in the next paragraph.

Boundary Conditions

Figure 13 shows that the calculation scheme requires values for $i_{max}+1$ and $i_{min}-1$. However, these do not exist. To obtain usable equations, substitution is essential.

Inside boundary

For a cylinder, the concentration at opposite points of the symmetry axis is always equal. For the inside boundary condition this implies:

$\frac{\delta C}{\delta r} = 0$ at i = 1 or $C'_{1,j} = 0$

This inside boundary is transferred to the same form as all inner nodes by applying a MacLaurin expansion. A MacLaurin expansion is a Taylor series around 0.

$$\frac{\delta C}{\delta r} = C'_{i,j} = C'_{1,j} + r \cdot C''_{1,j} + \frac{1}{2} \cdot r^2 \cdot C'''_{1,j} + \ldots \qquad (22)$$

Neglecting higher order terms and incorporating the fact that $C'_{1,j} = 0$ yields in:

$$\frac{1}{r} \cdot C'_{i,j} = C''_{1,j} \text{ or } \frac{1}{r} \cdot \frac{\delta C}{\delta r} = \frac{\delta^2 C}{\delta r^2} \qquad (22b)$$

With

$$\frac{\delta C}{\delta t} = D \cdot \frac{1}{r} \cdot \frac{\delta}{\delta r} \cdot \left(r \cdot \frac{\delta C}{\delta r} \right) = D \cdot \left(\frac{\delta^2 C}{\delta r^2} + \frac{1}{r} \cdot \frac{\delta C}{\delta r} \right) \Rightarrow \frac{\delta C}{\delta t} = 2D \cdot \frac{\delta^2 C}{\delta r^2} \qquad (22c)$$

which gives the solution:

$$\frac{\delta^2 C}{\delta r^2} = \frac{2\left(C_{0,j} - C_{1,j}\right)}{\delta r^2} \qquad (23)$$

because of symmetry over the inside boundary, $C_{0,j} = C_{2,j}$. Therefore, the fictive node $C_{0,j}$ can be substituted, resulting in:

$$\frac{\delta^2 C}{\delta r^2} = \frac{2\left(C_{2,j} - C_{1,j}\right)}{\delta r^2} \tag{23b}$$

So, yielding the finite difference form:

$$\frac{\delta C}{\delta t} = 2D \cdot \frac{2\left(C_{2,j} - C_{1,j}\right)}{\delta r^2} = \frac{4 \cdot D}{\delta r^2} \cdot \left(C_{2,j} - C_{1,j}\right) \tag{23c}$$

Outside boundary

For the surface boundary, a similar problem as for the inner boundary occurs. A point C_{imax+1} is introduced. This point does not exist, in addition to this, no symmetrical point exists either. To solve the problem, the mass transfer equation is used:

$$D \cdot \rho_w \frac{\delta C}{\delta x} = -k \cdot \left(p_p - p_a\right) \tag{24}$$

Therefore:

$$\frac{C_{i+1,j} - C_{i-1,j}}{2 \cdot \delta r} = \frac{-k}{D} \cdot \left(p_p - p_a\right) \Rightarrow C_{i+1,j} = C_{i-1,j} + \frac{2 \cdot \delta r \cdot -k}{D} \cdot \left(p_p - p_a\right) \tag{25}$$

Substitution results in:

$$\frac{C_{i,j} - C_{i,j-1}}{\delta t} = D \cdot \left(\frac{r_{i+0.5} \cdot \left[C_{i-1,j-1} + \frac{2 \cdot \delta r \cdot -k}{D} \cdot \left(p_p - p_a\right) \right] - \left(r_{i+0.5} + r_{i-0.5}\right) \cdot C_{i,j-1} + r_{i-0,5} \cdot C_{i-1,j-1}}{r_i \cdot \delta r^2} \right) \tag{25b}$$

Applying this equation requires conversion from surface water content to vapour pressure. Through the sorption isotherm [1], the water activity is calculated.

$$a_w = 1 - e^{\left(-5.18 * C^{0.93}\right)} \tag{3}$$

Water activity, in turn, is related to vapour pressure:

$$p_p = a_w \cdot p_{sat} \tag{4}$$

Air water content is calculated. The relationship between vapour pressure and concentration is defined for any gas by the ideal gas law:

$$p = \frac{n \cdot R \cdot T}{V} \qquad (26)$$

p is the pressure in Pa, V is the volume in cubic metres, T is the temperature in degrees Kelvin (degrees Celsius + 273.16), n equals the amount of gas in moles (1 mol H_2O = 0.018 kg), R is the gas constant: 8.314 Joules/mol/m^3.

To convert the water vapour pressure to concentration in kg/m^3:

$$p = \frac{\frac{x}{0.018} \cdot 8.314 \cdot T}{V} \qquad (26b)$$

So:

$$\frac{x}{V} = 0.002166 \cdot \frac{p_p}{T} = C_v \quad \text{in kgm}^{-3} \qquad (26c)$$

Since the conversion from vapour pressure to concentration produces different units, a translation needs to be made. In this case, this translation is easy. Division by the density of the product (water), yields a neutral SI unit.

$$\frac{C_v}{\rho_w} = C \qquad (\text{kgkg}^{-1} \text{ or } (-)) \qquad (26d)$$

Discretisation

Time and place discretisation are very important in applying a set of equations to model a process. In deciding between these figures for numerically iterative processes, the most common factors of importance is accuracy, followed by computation time.

Time step size

While it may be very advantageous to cut a process of several hours up into time steps of one hour as far as computation time is concerned, doing so may severely harm the accuracy of the simulation. On the other hand, time steps as low as fractions of a second will produce very accurate results, but drastically increases the time required for data collection. Ideally speaking, an infinite amount of iterations will produce an infinitely accurate simulation. Outside that ideal world, concessions need to be made. To investigate the limits of these concessions, maximum time step size is calculated.

The maximum size of a time step is limited by the size of the time constant (τ). Identification of the time constant is done by examining the core equations involved in the process. For the drying process under discussion the core equations are the (modified) diffusion equations.
For the inner nodes and surface boundary this gives:

$$\frac{dC}{dt} = \frac{C_{i,j} - C_{i,j-1}}{\delta t} = \frac{D}{\delta r^2} \cdot \left(\frac{r_{i+0.5}}{r_i} \cdot C_{i+1,j-1} - \frac{\left(r_{i+0.5} + r_{i-0.5}\right)}{r_i} \cdot C_{i,j-1} + \frac{r_{i-0,5}}{r_i} \cdot C_{i-1,j-1} \right) \tag{21c}$$

Which gives:

$$\tau_{i,s} = \frac{\delta r^2}{D} \tag{27}$$

(N.B. r_i is not taken up into the time constant, with adjustments of r_i, both $r_{i+0.5}$ and $r_{i-0.5}$ change accordingly. Values can just be considered constants, different for each layer.)

For the inside boundary this means:

$$\frac{dC}{dt} = \frac{C_{1,j} - C_{1,j-1}}{\delta t} = \frac{4 \cdot D}{\delta r^2} \cdot \left(C_{2,j} - C_{1,j}\right) \tag{23d}$$

Which gives:

$$\tau_c = \frac{\delta r^2}{4 \cdot D} < \tau_{i,s} \tag{28}$$

The highest stable time step for all points corresponds to τ_c.

For shrinking geometries, the time constant can become even smaller. With the aid of the shrinking equation (chapter 2), δr values can be compared over the entire drying range.

$$X(C_0) = X(10.4652) = 3479.6 : X(C_{end}) = X(0) = 1490.6$$
$$2.3344 : 1$$

For shrinking, this further reduces the maximum time step to $0.42 \cdot \tau_c$.

Accuracy assessment did not show considerable differences between simulation trials at dt = τ and dt = $0.05 \cdot \tau$ (figure 15). This is because the calculated value is an absolute minimum. In many occasions, the actual time step limitation may be higher. As far as accuracy and computation times are concerned, dt = τ is an acceptable relation.

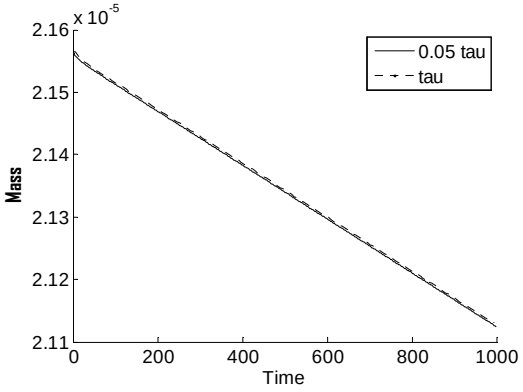

Figure 15. Time step size does not influence accuracy considerably.

Place step size

Determination of step size does not necessarily influence the model in accuracy and simplicity. Because the mass transfer coefficient is only represented in the surface boundary condition, the degree to which it influences the modeling process is related to the volume of the outside layer, or dr^2, $(\text{step size})^2$.

Because of other simplifications, estimated parameters will always need a conversion factor to be equal to actual values. The actual question is whether or not modification of the amount of layers will produce results that can be correlated to one another. If not, careful consideration is required.

To test the influence, four different datasets were investigated, using fitting, mass transfer coefficient values were found (k1 through k4). This process was repeated for different layer settings over the same dataset. The relative differences between the different layer settings were compared for each dataset. (figure 16). When these relative differences are compared to relative differences of other datasets, no significant differences are found.

From this, it can be derived that different layer settings affect different datasets equally. When trying to predict evaporation rates, a conversion factor can be applied. Since 3 layers produces the fastest parameter estimation, 3 layers will be used.

Table 8. Effect of place discretisation on various parameter estiamtions.

Layers	k 1	k 2	k 3	k 4
3	0.0012	0.002	0.0033	0.0011
5	0.0014	0.0023	0.0038	0.0012
10	0.0015	0.0024	0.004	0.0013

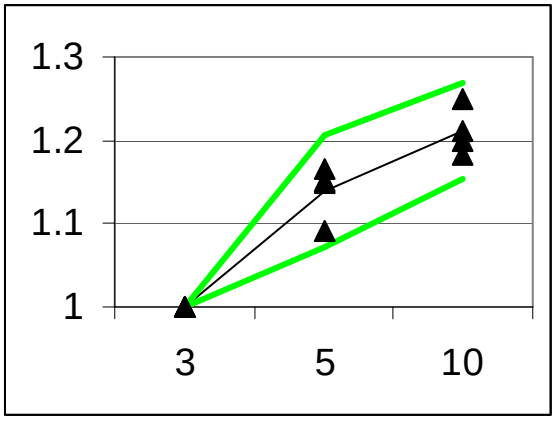

Figure 16. On the x-axis, the amount of layers. On the y-axis: coefficient values on a relative scale. Relative coefficient values are not significantly different, green lines represent higher and lower confidence interval.

5 Drying Simulation and Model Validation

A quick summary of the different approaches outlined in the previous paragraphs produces a number of possibilities for data fitting. Both standard and shrinking geometries for three different cylinder distributions offer 6 possible models available for obtaining the best fit.

Trial runs of the model featured manual boundary settings. Values for diffusion coefficients were set between $1*10^{-8}$ and $1*10^{-10}$ as realistic values.

All model fits produced typical curves (figure 17, 18).

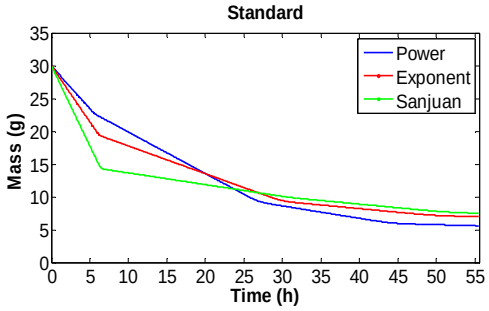

Figure 17, effect of different cylinder division on drying curve, non-shrinking.

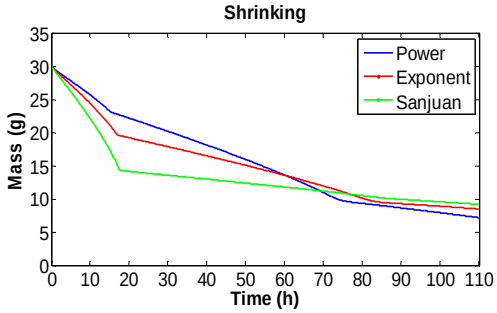

Figure 18, effect of different cylinder division on drying curve, shrinking.

While a set of measurements produces a smooth curve, the simulated data produce a rough range made up of 4 gradients. This is inherent to the sum of cylinder model. Smaller cylinders dry out much more quickly than large cylinders. Therefore, these small cylinders stop contributing to the drying process at an earlier point. The first change of gradient coincides with the moment small cylinders dry out. Division into more cylinders would produce a smoother line.

This is confirmation of the theory behind the model. An actual broccoli floret is not divided into 4 types of cylinders all of which have the exact same size. More likely, the size of these cylinders is normally distributed. In practice, this would yield a smooth line. The only limit of the model is a simplification.

As far as the different distributions are concerned, the Sanjuan distribution does not produce the signature drying curve and is unlikely to produce useful results. The exponential and power distribution look comparable at first glance. Testing will distinguish between the two.

The difference between a shrinkin and a non-shrinking model is mainly based on the duration of the process. Shrinking extends the duration of the process.

To find the most suitable model, diffusion and mass transfer rate coefficients were adjusted in data fits (appendix 3). The fit results were rated for their data-resemblance for different datasets. For these different datasets, drying parameters (flow rate, temperature and initial product mass) as well as drying duration were varied.

To this selection of datasets, all six models were applied. From the results, the top three fits were selected. This selection was done based on visual determination, much less on statistic accuracy. The reason for this is illustrated with an example: a straight line might fit better than another curve as far as the sum of squares is concerned, but if the trend of the residuals is ascending/descending away from the data curve, it is unlikely a better choice for the entire drying range. The selection is outlined in table 9.

Table 9. Model types that produce the best fits for different datasets.

Dataset	Top 3, alphabetical order		
Set 1	Shrinking, Power	Standard, Exponential	Standard, Power
Set 2	Shrinking, Power	Standard, Exponential	Standard, Power
Set 3	Shrinking, Power	Shrinking, Sanjuan	Standard, Power

In appendix 3, the best fits that were created are depicted. From this selection the power distribution appears to fit the situation very well. In addition to this, there is no remarkable difference between shrinking and non-shrinking models, aside from the obtained rate coefficients. Without a considerable contribution, additional complications of a model can not be justified. The simplified (standard) model was used.

6 Parameter Validation

Using a model without incorporation of shrinkage and a Power cylinder distribution, diffusion and evaporations parameters were estimated.
The diffusion rate coefficient does not deviate from the minimum restriction (1E-10), set by the operating function (appendix 1). Possibly the air flow rate is too low for sufficient water requirement at the surface: restriction by diffusion rate is never encountered, therefore the maximum diffusion rate is not achieved.
The mass transfer coefficient does show some variation, as shown in table 10. To determine the accuracy of these coefficient values, the variations are explained. The dependency of the mass transfer coefficient on processing conditions (air flow rate, and temperature) and product mass can be derived through the Sherwood number:

$$Sh = a \cdot \mathrm{Re}^{0.1} + \frac{b \cdot \mathrm{Re}^{0.7}}{1 + c \cdot \mathrm{Re}^{0.2}} \tag{29}$$

With

$$a = 0.462 \cdot Sc^{0.1} \qquad Sh = \frac{k \cdot L}{D_a}$$

$$b = \frac{2.5 \cdot Sc^{0.7}}{1 + 1.75 \cdot Sc^{5/12}} \quad \text{And} \quad Sc = \frac{\nu_a}{D_a}$$

$$c = 2.79 \cdot Sc^{0.2} \qquad \mathrm{Re} = \frac{\rho_a \cdot u \cdot L}{\eta}$$

Gives:

$$k = \frac{D_a}{L} \cdot 0.462 \cdot \left(\frac{\nu_a}{D_a}\right)^{0.1} \cdot \left(\frac{\rho_a \cdot u \cdot L}{\eta}\right)^{0.1} + \frac{2.5 \cdot \left(\frac{\nu_a}{D_a}\right)^{0.7}}{1 + 1.75 \cdot \left(\frac{\nu_a}{D_a}\right)^{5/12}} \cdot \left(\frac{\rho_a \cdot u \cdot L}{\eta}\right)^{0.7}}{1 + 2.79 \cdot \left(\frac{\nu_a}{D_a}\right)^{0.2} \cdot \left(\frac{\rho_a \cdot u \cdot L}{\eta}\right)^{0.2}} \tag{29b}$$

In this equation, L (characteristic length) is influenced by mass, u (air velocity) is influenced by air flow rate and ν_a (kinematic viscosity), D_a (water vapour diffusion coefficient), ρ_a (air density) and η (dynamic viscosity of air) are influenced by temperature (appendix 2).
Calculating the theoretical mass transfer coefficient and comparing against fitted results can help explaining variance, and therefore determine the reliability of the model.

Table 10. Acquired mass transfer coefficients, according to the power distribution.

	Data 1	Data 2	Data 3
Initial mass (g)	34.56	26.88	23.25
Temperature (C)	24	35	53
Air flow rate (ms^{-1})	0.23	0.23	0.025
k, measured	0.0012	0.0021	0.0031
k, predicted	0.054	0.062	0.029

To find out about the coherence of these coefficients, the explained variance in a linear relationship was investigated (figure 19). In this investigation the coherence is disappointing. Because a linear relation was expected, the y-intercept of the linear correlation was set at 0. This yielded a negative correlation (R^2 = -1.6022). From further testing, this result was appointed to the effect of air flow rate.

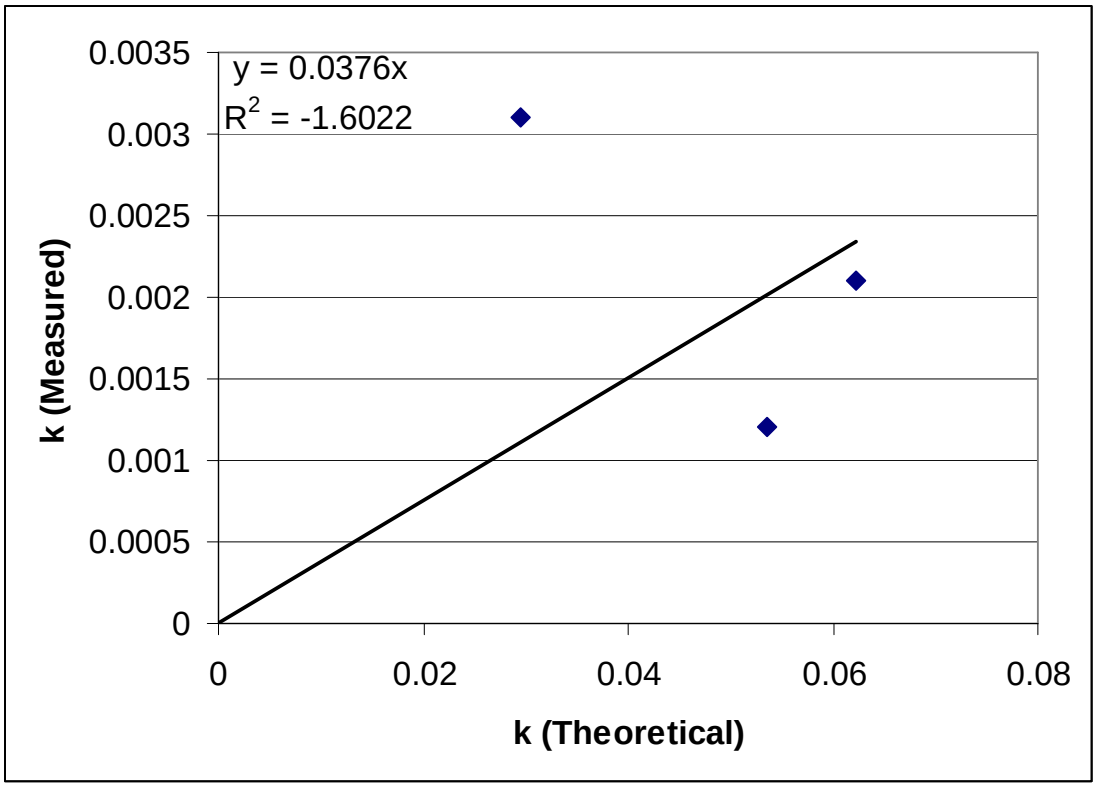

Figure 19. Negative correlation between theoretical and approximated mass transfer coefficient.

When running more experiments while keeping the air flow rate constant, the results gathered from fitting of data linearly cohered with the predicted data (figure 20). From this it can be concluded that the model works. However, the air flow patterns inside the dryer should be thoroughly investigated in order to predict accurate values for different air flow rates.

Table 11. Acquired mass transfer coefficients, according to the power distribution.

	Data 1	Data 2	Data 5
Initial mass (g)	34.56	26.88	14.8
Temperature (C)	24	35	25.28
Air flow rate (ms^{-1})	0.23	0.23	0.23
k, measured	0.0012	0.0021	0.0028
k, predicted	0.054	0.062	0.088

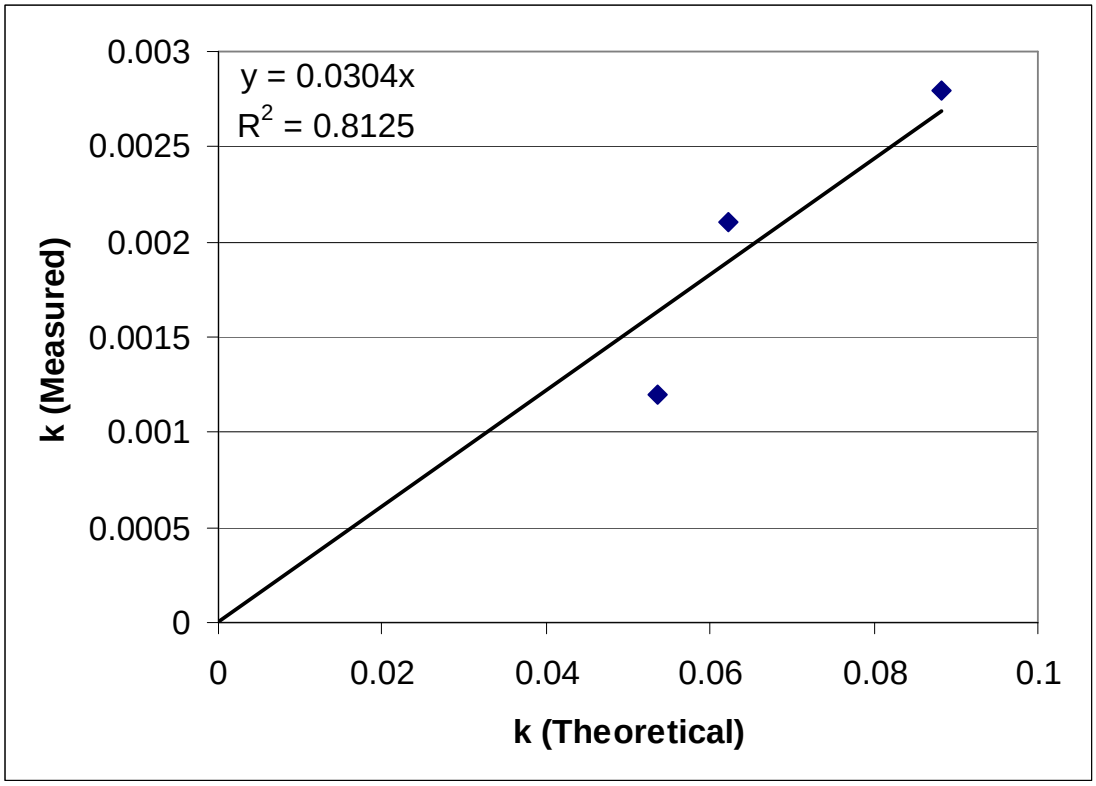

Figure 20. Positive correlation between theoretical and approximated mass transfer coefficient.

The relation between estimated and theoretical values is established:

$$k_t = 0.0304 \cdot k_m \qquad (30)$$

With k_t as theoretical value and k_m as estimated (measured/fitted) value.
To check the accuracy of this relation, a reverse simulation was performed:
For the starting condition of a drying process, the theoretical evaporation rate coefficient is calculated. This value is translated to a value that is suitable for simulation through equation 30. In addition to this, an estimated heat transfer coefficient is applied. Combining these values, a drying process was simulated.
This simulation is compared against the actual (measured) drying process in figure 21.

Table 12. Values for simulation of a measured broccoli sample.

Temperature air	~ 35.29
Temperature product (t = 0)	20
Mass product (t = 0)	26.88
Air flow rate	0.23
k_t	0.062
k_m	0.00189
h_m (measure)	0.0044
h_m (estimate)	0.0048

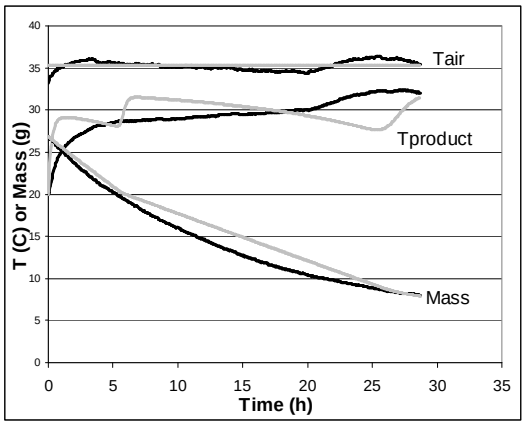

Figure 21. Comparison of simulated and measured results, calculated through the heat transfer coefficient.

The similarity between theoretical and measured values give a good indication of the ultimate validity of the model. In this case, the correlation between model and measured data is quite good.

7 Conclusion

Modelling of the convection drying process of a broccoli floret can be done using one dimensional diffusion schemes. Using a multi cylinder model on experimental data, mass transfer rate coefficients were found that cohered with theoretical values at constant air flow rates.

In this work it was found that incorporation of shrinkage into the model does not contribute significantly to the accuracy of the outcome. However, definite shrinkage was identified. Possibly, shrinking of organic, living materials is not modelled according to basic physics. Other options of different shrinkage modelling can also be thought of (e.g. less dimensions). This may lead to further sophistication of the model.

Inside typically large broccoli florets (> 40g) no considerable contribution of temperature gradients to reaction rates was found. For broccoli drying, temperature gradients can therefore be ignored.

It was found that the complex structure of the broccoli floret does not inhibit estimation of rate coefficients dependent on surface area. Instead, mass can be used as an indicator of surface area. With this, problems like heat conduction, could be solved. Therefore, consistency of shape between different florets and for shrunk florets is valid.

During fitting, the effect of the air flow rate could not be predicted. Perhaps this is because only low air flow rates were considered in combination with the nature of the experimental setup. Perhaps some research on high air flow rates (up to 2.5 ms^{-1}) could give more information on this mechanism.

All together, transferring theoretical values through simple linear relations to values suitable for modelling, the drying curve of a complicated structure like a broccoli floret over several hours can be predicted employing a multi-cylinder conversion of Fick's second law on diffusion.

8 References

1. Mulet A., Sanjuán N., Bon J., Simal S., Eur Food Res Technol 210 (1999), 80–83.
2. Ratti C., Crapiste C.H., Journal of Food Process Engineering 18 (1995), 41-53.
3. Woods D.R., Rules of Thumb in Engineering Practice 2007
4. Sanjuán N., Cárcel J.A., Clemente G., Mulet A., Eur Food Res Technol 212 (2001), 449–453.
5. Gutierrez-Miravete E., conduction heat transfer, 2002
6. Hewlett Packard, Practical Temperature Measurements, Application Note 290 (1980).
7. Sweat V.E., Journal of Food Science 39 (1974), 1080-1083
8. Burdurlu H.S., Koca N., Karadeniz F., Journal of Food Engineering 74 (2006), 211–216.
9. Spang B., Correlations for Convective Heat Transfer, http://www.cheresources.com.

Appendix

Appendix 1 MATLAB file

Standard function

```
function [M,tijd]=Cylinder1(k,D,R,h,tend)
cons=1;
rhodm=1120;rhow=1000;V0=1;wat=92.139;Vw=V0*wat/100;Vdm=V0-
Vw;dm=Vdm*rhodm;C0=Vw*rhow/(dm);h0=h;
rho0=(C0*dm+dm)/((C0*dm)/rhow+dm/rhodm);
psat=7325;
pa=0.15*psat; %RH=10
L=3;%amount of layers (2 boundary + L-2 inner)

F=(0.005/3)^2/118;%constant F, for approximating time constant
y=round(tend/(((R/L)^2/F)/100));%Ensuring divisibility by dt
dt=(tend/y);
if dt>10
    dt=10;
end
jmax=tend/dt;dr=R/L;imax=R/dr;
T=24;

%time discretisation
for j=1:jmax;
time(j)=(j*dt)-dt;
end

%place discretisation
for i=1:imax+1;
r(i)=(i*dr);
end

%initial conditions
for i=1:imax;
C(i,1)=C0;
pp(1)=psat;
h(i)=h0;
m(1,1)=pi*r(1)^2*h0*(C0*dm+dm);
m(i,1)=pi*(r(imax-1)^2-r(1)^2)*h0*(C0*dm+dm);
m(imax,1)=pi*(r(imax)^2-r(imax-1)^2)*h0*(C0*dm+dm);
rho(1)=rho0;
end

%nodes
for j=2:jmax;
%core
C(1,j)=C(1,j-1)+((D*4*dt)/((dr)^2))*(C(2,j-1)-C(1,j-1));
m(1,j)=pi*r(1)^2*h(1)*(C(1,j)*dm+dm);
%inner nodes
    for i=2:imax-1;
C(i,j)=C(i,j-1)+((D*dt)/(r(i)*(dr)^2))...
    *(0.5*(r(i)+r(i+1))*C(i+1,j-1)-...
    (0.5*(r(i)+r(i+1))+0.5*(r(i)+r(i-1)))*C(i,j-1)+ ...
    0.5*(r(i)+r(i-1))*C(i-1,j-1));
m(i,j)=pi*(r(i)^2-r(i-1)^2)*h(i)*...
    (C(i,j)*dm+dm);
if i>2
```

```
m(i,j)=m(i,j)+m(i-1,j); %+summation term
end
    end
%surface
pp(j)=(1-exp(-5.18*(C(imax,j-1))^0.93))*psat; %sorption isotherm
C(imax,j)=C(imax,j-1)+((D*dt)/(r(imax)*(dr)^2))...
    *(0.5*(r(imax)+r(imax+1))*...
    (C(imax-1,j-1)+((2*-(cons*k)*(dr))/D)*((0.002166*...
    (pp(j)-pa))/(T+273.16))/rhow)-(0.5*(r(imax)+r(imax+1))...
    +0.5*(r(imax)+r(imax-1)))*C(imax,j-1)...
    +0.5*(r(imax)+r(imax-1))*C(imax-1,j-1));
m(imax,j)=pi*(r(imax)^2-r(imax-1)^2)*h(imax)*...
    (C(imax,j)*dm+dm);
end
M=m(1,:)+m(imax-1,:)+m(imax,:);
```

Shrinking function

```
function [M,time]=Cylinder2(k,D,R,h,tend)
cons=1;
rhodm=1120;rhow=1000;V0=1;wat=92.139;Vw=V0*wat/100;Vdm=V0-
Vw;dm=Vdm*rhodm;
C0=Vw*rhow/(dm);h0=h;
rho0=(C0*dm+dm)/((C0*dm)/rhow+dm/rhodm);
psat=7325;pa=0.15*psat; %RH=10
L=3;%amount of layers (2 boundary + L-2 inner)
F=(0.005/3)^2/118;%constant F, for approximating time constant
y=round(tend/(((R/L)^2/F)/3));%Ensuring divisibility by dt
dt=(tend/y);
if dt>10
    dt=10;
end
jmax=tend/dt;dr=R/L;imax=R/dr;T=35;

%time
for j=1:jmax;
time(j)=(j*dt)-dt;
end

%place
for i=1:imax+1;
r(i,1)=(i*dr);
end

%initial conditions
for i=1:imax;
C(i,1)=C0;
pp(1)=psat;
h(i,1)=h0;
V(i,1)=V0;
X(i,1)=(V(i,1)/(pi*r(i,1)^2*h0))^(1/3);
m(1,1)=pi*r(1)^2*h0*rho0;
m(i,1)=pi*(r(imax-1,1)^2-(r(imax-1,1)-(i-1)*dr)^2)*h0*rho0;
m(imax,1)=pi*(r(imax,1)^2-(r(imax,1)-dr)^2)*h0*rho0;
rho(1)=rho0;
end

%nodes
for j=2:jmax;
```

```
%core
V(1,j)=((C(1,j-1)*dm)/rhow+dm/rhodm);
X(1,j)=((V(1,j)/(pi*r(1,1)^2*h0))^(1/3))/X(1,1);
r(1,j)=r(1,1)*X(1,j);
h(1,j)=h0*X(1,j);
C(1,j)=C(1,j-1)+((D*4*dt)/((X(1,j)*dr)^2))*(C(2,j-1)-C(1,j-1));
m(1,j)=pi*r(1,j)^2*h(1,j)*...
    (C(1,j)*dm+dm)/(C(1,j)*dm/rhow+dm/rhodm);
%inner nodes
    for i=2:imax-1;
V(i,j)=((C(i,j-1)*dm)/rhow+dm/rhodm);
X(i,j)=(V(i,j)/(pi*r(i,1)^2*h0))^(1/3)/X(i,1);
r(i,j)=r(i,1)*X(i,j);
h(i,j)=h0*X(i,j);
C(i,j)=C(i,j-1)+((D*dt)/(r(i,j)*(X(i,j)*dr)^2))...
    *(0.5*(r(i,j)+r(i+1,j))*C(i+1,j-1)-...
    (0.5*(r(i,j)+r(i+1,j))+0.5*(r(i,j)+r(i-1,j)))*C(i,j-...
    1)+0.5*(r(i,j)+r(i-1,j))*C(i-1,j-1));
m(i,j)=pi*(r(i,j)^2-(r(i,j)-X(i,j)*dr)^2)*h(i,j)*...
    (C(i,j)*dm+dm)/(C(i,j)*dm/rhow+dm/rhodm);
if i>2
m(i,j)=m(i,j)+m(i-1,j); %+summation term
end
    end
%surface
V(imax,j)=((C(imax,j-1)*dm)/rhow+dm/rhodm);
X(imax,j)=(V(imax,j)/(pi*r(imax,1)^2*h0))^(1/3)/X(imax,1);
r(imax,j)=r(imax,1)*X(imax,j);
h(imax,j)=h0*X(imax,j);
pp(j)=(1-exp(-5.18*(C(imax,j-1))^0.93))*psat;%sorption isotherm
C(imax,j)=C(imax,j-1)+((D*dt)/(r(imax,j)*(X(imax,j)*dr)^2))...
    *(0.5*(r(imax,j)+r(imax+1,j))*(C(imax-1,j-1)+((2*-...
    (cons*k)*X(imax,j)*(dr))/D)*((0.002166*(pp(j)-pa))/(T+273.16)...
    )/rhow)-(0.5*(r(imax,j)+r(imax+1,j))+0.5*(r(imax,j)+r(imax-...
    1,j)))*C(imax,j-1)+0.5*(r(imax,j)+r(imax-1,j))*C(imax-1,j-1));
m(imax,j)=pi*(r(imax,j)^2-(r(imax,j)-X(imax,j)*dr)^2)*h(imax,j)*...
    (C(imax,j)*dm+dm)/(C(imax,j)*dm/rhow+dm/rhodm);
end
M=m(1,:)+m(imax-1,:)+m(imax,:);
```

Operating function

```
function [MT]=Drying(beta0,I)

% Determine Sequence Length and initial Mass
load data.txt
data=data(1:(1/1)*end);
m0=mean(data(1:10))/1000;
tend=length(data)/10;

% Amount of florets
N=1;

% Cylinder division
a1=2209.65*N;a2=24.69888*N;a3=9.935957*N;a4=1*N;%copy
% a1=1344.261405*N;a2=121.8023928*N;a3=11.03641213*N;a4=1*N;%Exponent
% a1=876.6152703*N;a2=214.8428876*N;a3=29.60768938*N;a4=1*N;%power

rho0=1009.4;t=0.064/1.75;u=0.85/0.875;v=0.31/1.75;
w=0.47/0.875;x=0.51/1.75;y=0.74/0.875;z=1.23/0.875;
r4=(m0/(pi*rho0*(a1*t^2*u+a2*v^2*w+a3*x^2*y+a4*z)))^(1/3);
h4=(r4*z);r1=r4*t;r2=r4*v;r3=r4*x;
h1=(0.85/1.23)*h4;h2=(0.47/1.23)*h4;h3=(0.74/1.23)*h4;

%guess values
D=beta0(2);k=beta0(1);

%limits
if D<=1*10^-10;
    D=1*10^-10;
elseif D>1*10^-8;
    D=1*10^-8;
end

% calculation cylinder masses
% [M,time]=Cylinder1(k,D,r1,h1,tend);M1=interp1(time,M,[1:10:tend]);
% [M,time]=Cylinder1(k,D,r2,h2,tend);M2=interp1(time,M,[1:10:tend]);
% [M,time]=Cylinder1(k,D,r3,h3,tend);M3=interp1(time,M,[1:10:tend]);
% [M,time]=Cylinder1(k,D,r4,h4,tend);M4=interp1(time,M,[1:10:tend]);
 [M,time]=Cylinder2(k,D,r1,h1,tend);M1=interp1(time,M,[1:10:tend]);
[M,time]=Cylinder2(k,D,r2,h2,tend);M2=interp1(time,M,[1:10:tend]);
[M,time]=Cylinder2(k,D,r3,h3,tend);M3=interp1(time,M,[1:10:tend]);
[M,time]=Cylinder2(k,D,r4,h4,tend);M4=interp1(time,M,[1:10:tend]);

% Calculate total mass
MT=a1*M1+a2*M2+a3*M3+a4*M4;
MT=MT';
```

Appendix 2 Influence of Process Parameters on Process Rates

L

According to the power-cylinder division, each mass is assigned 4 cylinder sizes. Each of these cylinders has its own characteristic dimension (V/A=L). The total characteristic dimension of a broccoli floret will be determined according to the value for each different cylinder multiplied by its contribution to the total mass. Even though this method may not be entirely correct, it does produce relatively different figures.

Example:
Cylinder 1 has a characteristic dimension of 2 and all 22 of these cylinders combined make up 30% of the floret mass. Its contribution to the total dimension (its contribution figure) equals 2*30/100=0.6. The sum of the contribution figures of all cylinders gives the total characteristic dimension.

From calculations of actual figures, the relation L = 0.0003*mass - 4E-06 was derived.

u

The air flow rate measurements done in the experimental setup are converted to air velocities.

v_a

Determined according to the engineering toolbox
[http://www.engineeringtoolbox.com/air-absolute-kinematic-viscosity-d_601.html]

D_a

Values for the vapour diffusion coefficient are determined according to the method described in R. Bolz and G. Tuve, Handbook of tables for applied engineering science. (2nd ed.),, CRC Press, Cleveland (1976).

ρ_a

Determined according to James A. Ierardi
(http://users.wpi.edu/~ierardi/PDF/air_density_plot.PDF)

η

Determined according to Spyros A. Kinnas,
http://www.ce.utexas.edu/prof/kinnas/319LAB/Book/CH1/PROPS/dynviscgif.html

Appendix 3 Data Fitting

For dataset 1, the top three in alphabetic order were.

- Shrinking, P-distributed:

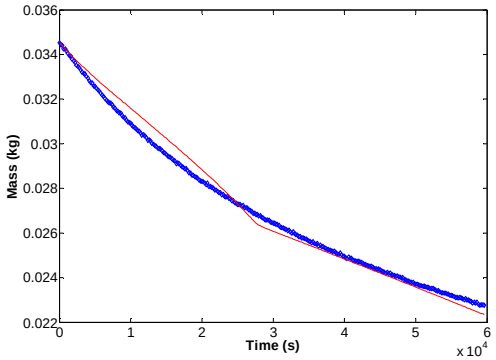

- Standard, E-distributed:

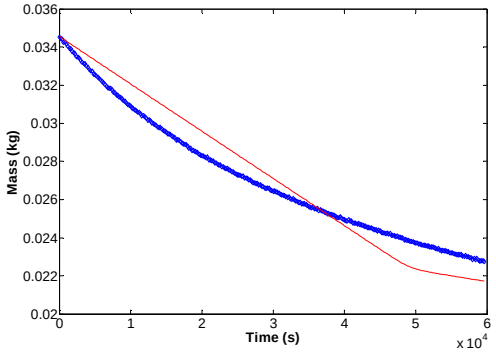

- Standard, P-distributed:

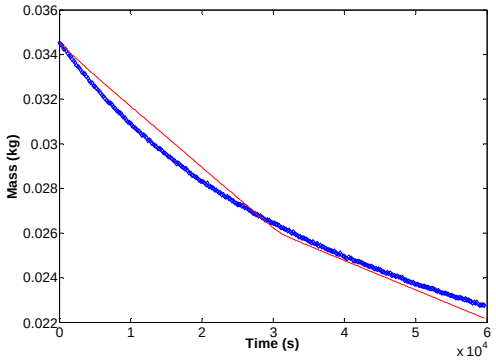

For dataset 2 the top three in alphabetic order were.

- Shrinking, P-distributed:

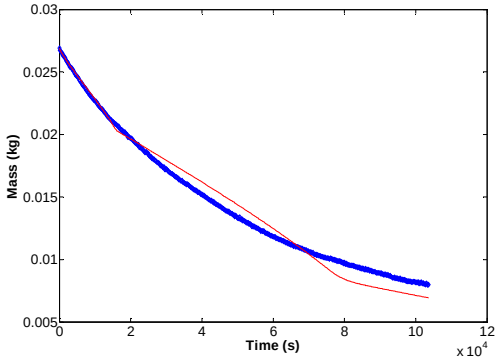

- Standard, E-distributed:

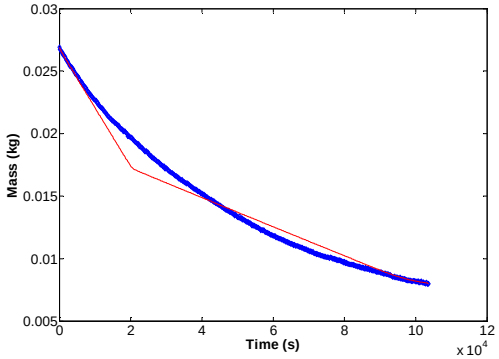

- Standard, P-distributed:

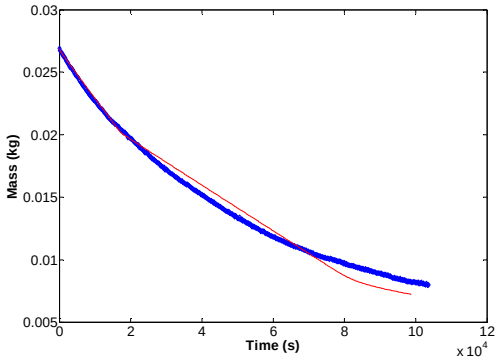

For dataset 3 the top three in alphabetic order were.

- Shrinking, P-distributed:

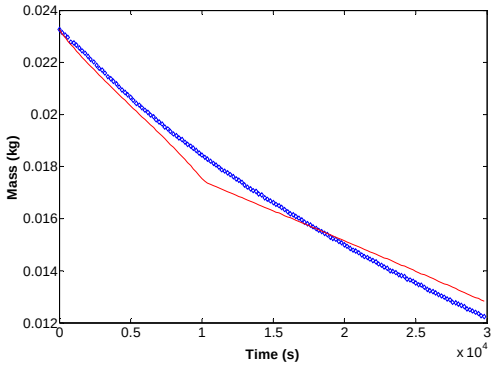

- Shrinking, S-distributed:

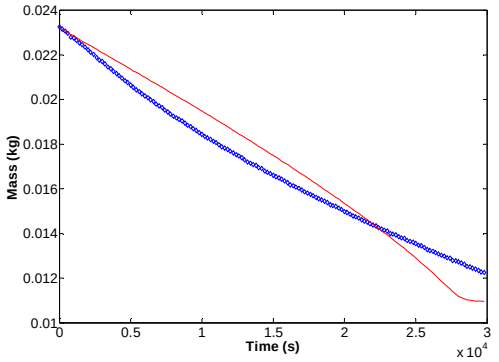

- Standard, P-distributed: